Identification of Drug Targets and Potential Molecular Mechanisms of Wantong Jingu Tablet in Treatment of Rats with Collagen-Induced Arthritis based on 16S rDNA High-Throughput Sequencing and Metabolomic Analysis

Zhaodong Li
Jilin University

Fangyuan Qi
Jilin University

Fan Li (✉ lifan@jlu.edu.cn)
Jilin University

Research

Abstract

Background: Wantong Jingu Tablet (WJT), a mixture of traditional Chinese medicine, can reduce the symptoms of rheumatoid arthritis (RA), but its pharmacological mechanism is unclear. The aims of this study were to investigate the therapeutic mechanisms of WJT for RA in vivo.

Methods: The effects of WJT on the joint pathology, and the levels of Bax, Bcl-2,caspase-3, cleaved-caspase-3, ERK1/2, pERK1/2, TNF-α, IL-1β, and IL-6 were demonstrated based on several experiments in the model of collagen-induced arthritis (CIA) in rats. 16S rDNA high-throughput sequencing was used to investigate the effect of WJT on the overall structure and composition of gut microbiota. Meanwhile, metabolite changes in faeces were analyzed by metabolomics techniques.

Results: The results showed that WJT restored the joint pathology in CIA rats, upregulated Bax and cleaved-caspase-3, downregulated Bcl-2, caspase-3, and pERK1/2, and reduced the levels of pro-inflammatory cytokines. The overall gut microbial structure in CIA rats was altered after WJT treatment. Three bacterial phyla were prominently restored: *Bacteroidetes*,*Tenericutes* and *Deferribacteres,* and three bacterial genera were significantly reversed: *Vibrio*, *Macrococcus* and *Vagococcus*. Furthermore, five specific metabolites associated with these specific bacterial genera were identified by correlation analysis. In addition, WJT supplement trended to down-regulate the other five metabolites according to metabolomic analyses.

Conclusions: These results revealed that WJT restored the pathological changes of RA might through activating the mitochondrial apoptosis pathway, inhibited MEK/ERK signaling, and modulating the special bacteria and the special metabolites.

Background

Rheumatoid arthritis (RA) is a chronic, systemic, autoimmune disease characterized by joint inflammation and synovial hyperplasia, and research indicates an increasing prevalence of RA worldwide [1]. In RA, a large number of immune cells, T cells, B cells and macrophages, are present in the infamed synovium [2]. Recruited T cells activate B cells, macrophages, and fibroblasts to create a complex network of various secreted cytokines, such as TNF-α, IL-1β and IL-6, thereby maintaining synoviocytes in an activated and infamed state [3, 4]. Moreover, increased concentrations of TNF-α, IL-1β, and IL-6 in the synovium lead to varying degrees of bone resorption and joint destruction [4, 5]. There are no structure-modifying drugs or optimal treatments available for RA. Thus, there is an urgent need for novel, cost-effective, and safe anti-infammatory therapies for the treatment of RA.

Wantong Jingu Tablet (WJT), the prescription drug approved by the Chinese government for RA treatment (Approval Number: Z20025183), is an herbal compound containing 25 herbal medicines with many pharmaceutical effects. It exerted curative effects on treating cervical spondylotic myelopathy, a serious degenerative disease, and the total effective rate was up to 83.3% [6]. Recently, a study has found that WJT had clinical curative effect in treatment of periarthritis, significantly relieving shoulder

pain and improving shoulder function [7]. Moreover, WJT could protect against collagen-induced arthritis in rats by disturbance of gene expression levels and induction of synoviocy tes apoptosis [8]. These studies suggest that WJT has pharmaceutically potential roles in restoring the pathogenesis and progression of RA.

Recent studies on the therapeutic mechanisms of herbal medicines have focused on alterations in gut microbial communities [9]. Some studies have demonstrated that herbal medicines effectively treat diseases and also regulate the structure and composition of intestinal flora [10]. Metabolomics is another emerging high-throughput technique that comprehensively analyzes endogenous small metabolites in organisms, and can identify novel molecular markers and potential therapeutic targets [11]. Furthermore, the rat CIA model is widely used for the study of joint inflammation because of its low mortality and characteristics by mimicing the progression and pathological phenomena of human RA [12, 13].

Accordingly, the aims of this work are to determine the effect of WJT on the production of pro-inflammatory cytokines, namely TNF-α, IL-1β, and IL-6, in the serum and joint tissue of rats. More specifically, we used different omics technologies to identify potential molecular mechanisms and pharmacological targets of WJT in the therapy of RA.

Materials And Methods

Preparation of samples

Samples of WJT powder were provided by Jilin Wantong Pharmacy Group Company (Tonghua, China). The traditional Chinese medicine containing in WJT was indicated in **Supplymentary Table S1**.

Acute toxicity in rats

One hundred and twenty female specific pathogen free (SPF) Sprague-Dawley (SD) rats weighing 160 to 180g were obtained from Changchun Yisi Experimental Animal Technology Company. The rats were randomly assigned to six groups (G1, G2, G3, G4, G5, and G6), fasted for 12 h, but with free access to drinking water, before a single administration of 1 g (G1), 2 g (G2), 3.98 g (G3), 7.94 g (G4), 15.85 g (G5), 31.62 g (G6) of WJT power per kg of body weight. Signs of toxicity were evaluated based on mortality. On day 14, survival rates were measured and the LD_{50} value was calculated based on the Improved Koch's method.

The rats were anaesthetised with an intraperitoneal injection of 10% pentobarbital sodium (4 ml/kg) and subsequently sacrificed by rapid decapitation. All animal experiments were approved by the Animal Research Committee of Jilin University. The principles in the ARRIVE guidelines and the Basel declaration (http://www.basel.declaration.org) have been considered when planning the experiments.

Induction of collagen-induced arthritis (CIA) in rats

Fifty female SPF SD rats were randomly divided into five groups after acclimatization for 1 week: control (no CIA), model (CIA alone), CIA + 150 mg/kg WJT, CIA + 300 mg/kg WJT, and CIA + 600 mg/kg WJT, with 10 rats per group. CIA in rats was conducted according to previously described by Jian Zuo et al. [14]. Then, rats in three WJT groups were given oral WJT solution (150, 300, or 600 mg/kg) each day starting on day-1; rats in control and model groups were given the same volume of normal saline. All rats were sacrificed on day-28 for further study.

Assessment of arthritis severity

On day 28, paw swelling and paw thickness were measured using a plethysmometer and an electronic vernier caliper, respectively. The severity of arthritis was evaluated using an arthritis index (AI) with a CIA semi-quantitative scoring system, as previously described by Nagaraja Haleagrahara et al. [15].

Measurement of inflammatory factors

On day 28, paw and ankle tissues were collected and broken apart using a homogenizer (JinXin, Shanghai, China) at 4 °C for collection of tissue fluid. The tissue fluid and blood were then centrifuged, and the supernatant was analyzed for the levels of pro-inflammatory factors (TNF-α, IL-1β, and IL-6) using enzyme linked immunosorbent assay (ELISA) kits (Abcom, Cambridge, UK), following the manufacturer's protocols.

Histopathological evaluation of ankle joints

After fixation, the tissue samples were processed, embedded in paraffin, and then cut into 4 mm slices using a microtome (Leica, Shanghai, China). Microscopic changes of the ankle joints were visualized using a light microscope (Olympus, Japan) after hematoxylin and eosin (H&E) staining. The severity of pathological changes in the ankle joints was measured according to previously described by Acharya Balkrishna et al. [16].

Immunohistochemical analyses

The paraffin-embedded samples of the ankle joints were blocked by 5% bovine serum albumin (BSA; Solarbio, Beijing, China) for 30 min, incubated with an appropriate primary antibody from Abcom (Cambridge, UK) overnight at 4°C, and then with a secondary antibody (Bioss, Beijing, China) at room temperature for 30 min. Enhancement was performed using a DAB dye solution and counter staining with hematoxylin. Finally, the ankle samples were observed under a light microscope (Olympus) at 400×, and

typical images are presented. Image analysis software (Image Pro Picture) was used for quantitative analysis.

Western blot analysis

After quantification of total protein extracted from knee and ankle synovia, equal amounts of protein lysates (20 μg per lane) were separated by 8-12% SDS-PAGE gels, and then transferred to 0.45 μm polyvinylidene fluoride (PVDF) membranes (ThermoFisher, Waltham, MA, USA). The membranes were blocked using 5% BSA, and then incubated with antibodies against Bax, Bcl-2, caspase-3, cleaved-caspase-3, MEK, pMEK, ERK1/2, pERK1/2, and β-actin (all from Abcom) at 4 °C overnight. Then, the PVDF membranes were treated with a horseradish peroxidase-conjugated secondary antibody (Bioss) at room temperature for 2 h. Protein bands were visualized on a Tanon 5200 Chemiluminescent Imaging System (Tanon, Shanghai, China).

Sequencing and data analysis

Sequencing and data analysis were performed following the manufacturer's guidelines by Novogene bio-information technology Co., Ltd, as previously described by Jing Wang et al. [17].

Metabolism and data analysis

On day-28, blood samples from sacrificed CIA rats were centrifuged at 4000 rpm (4°C for 5 min), and the supernatant was diluted with methanol so the final methanol concentration was 60% by use of liquid chromatograph-mass spectrometer (LC-MS) grade water. Then, the samples were transferred to fresh Eppendorf tubes with 0.22 μm filters, and centrifuged at 15,000 g (4°C for 10 min). Finally, the filtrate was subjected to LC-MS/MS analysis using a Vanquish UHPLC system (Thermo Fisher, Waltham, USA) coupled with an Orbitrap Q Exactive series mass spectrometer (Thermo Fisher).

The raw data files generated by UHPLC-MS/MS were processed and normalized using Compound Discoverer version 3.1 (Thermo Fisher). Statistical analyses were performed using the R software package (version 3.4.3), Python (version 2.7.6), and CentOS (release 6.6). Then the normalized data were matched with the mzCloud (https://www.mzcloud.org) and ChemSpider (http://www.chemspider.com/) databases to obtain the accurate qualitative and relative quantitative metabolism results. Principal co-ordinates analysis (PCoA) was performed using metaX (http://metax.genomics.cn). Univariate analysis was used with the t-test to calculate statistical significance (P-value). All metabolites with a variable importance in projection (VIP) greater than 1, a P-value below 0.05, and a fold change (FC) of 2 or more or 0.5 or less or were considered to be differentially regulated metabolites. The screened out metabolites were finally visualized as volcano plots, heatmaps, and mapped onto KEGG pathways.

Statistical analysis

Except the 16S rDNA high-throughput sequencing and metabolomics, data are presented as means ± standard deviations (SDs). Student's t-test was used to compare groups, and all statistical analyses were conducted using SPSS version 20.0. All experiments were performed at least three independent times. Differences were considered to be statistically significant at $p < 0.05$ and highly significant at $p < 0.01$.

Results

Acute toxicity assay

To determine the appropriate doses of WJT for rats, we initially performed an acute toxicity assay (**Figure 1A**). The median lethal dose (LD_{50}), calculated using the Improved Koch's method, was 6.24 g/kg, and the 95% confidence interval was 4.16 to 9.34 g/kg. In this work, the maximum drug dose is one-tenth of the LD_{50}. Therefore, the drug doses of WJT were 600 mg/kg, 300 mg/kg, and 150 mg/kg for further study. The H&E staining results indicated that WJT treatment exhibited no evident damage to the liver, spleen, and kidney of rats (**Figure 1B**).

WJT inhibited paw swelling in CIA rats

A significant increase in paw volume was shown after CIA immunization (**Figure 1C**). However, the paw edema was obviously reduced after oral administration of WJT at 300 and 600 mg/kg/day compared to model group. The arthritis index, paw thickness, and paw swelling decreased significantly in a dose-dependent manner (**Figure 1D**).

WJT reversed pathological changes in CIA rats

Histopathological results found that normal rats exhibited clear and complete histological architecture of the ankle joints (**Figure 1E**). But CIA rats had abnormal histological architecture in the ankle joints, with manifestations of synovial hyperplasia, massive inflammatory cells infiltration, pannus formation, and cartilage and bone erosion. By comparison, WJT alleviated these pathological conditions a lot. Synovial hyperplasia, infiltration of inflammatory cells and erosion of synovial tissues were obvious suppressed after oral administration of WJT at 600 mg/kg/day (**Figure 1F**).

WJT activated the mitochondrial apoptosis pathway and inhibited MEK/ERK signaling in synovial tissues

Compared to the CIA rats, the protein levels of Bax and cleaved-caspase-3 were prominently increased after WJT treatment, and down-regulation of Bcl-2 and caspase-3 was observed following WJT

supplement (**Figure 2A**). In addition, the expression levels of MEK, pMEK, ERK, and pERK were prominently up-regulated in CIA rats compared to the normal rats. However, WJT supplement (600 mg/kg) significantly reversed these proteins expression (**Figure 2B and C**).

WJT suppressed the levels of pro-inflammatory cytokines in serum and ankle joints

The levels of TNF-α, IL-1β, and IL-6 in serum and ankle joints were shown in **Figure 3.** Compared with the control group, the levels of these pro-inflammatory cytokines were markedly up-regulated in CIA rats. However, treatment with WJT (600 mg/kg) down-regulated TNF-α, IL-1β, and IL-6 levels compared to CIA rats.

WJT changes the overall structure of gut microbiota

The intestinal flora structures of rats in control, model, and 600 mg/kg WJT treatment groups were investigated by 16S rDNA sequencing. There were 714 differential operational taxonomic units (OTUs) in all three groups, and 14, 51 and 420 unique OTUs were examined in the control, model, and WJT treatment groups, respectively (**Supplymentary Figure S1**). WJT significantly changed the Chao index and Shannon index, selected for the alpha diversity of the gut microbiota. PCoA plot and UPGMA clustering tree found that rats among the three groups had different overall structures of the bacterial communities.

WJT modulates the composition of gut microbiota

The histograms and the clustering map illustrating the community structure of gut microbiota revealed the dominant microbial species and their relative abundance at the phylum level (**Figure 4A**). WJT supplement significantly reduced the abundances of *Bacteroidetes*, *Tenericutes* and *Deferribacteres* compared to the CIA rats (**Figure 4B**). *Firmicutes* and *Bacteroidetes* were the two most abundant bacterial phyla in the gut microbiota community. Compared to the normal rats, the ratio of *Firmicutes* to *Bacteroidetes* was markedly increased in CIA rats, whereas WJT treatment significantly reversed the ratio (**Figure 4C**).

At the genus level, the top 35 abundant bacterial genera among the three different groups were displayed by histograms and clustering map (**Figure 4D**). The proportion of *Vibrio*, *Macrococcus* and *Vagococcus* was markedly up-regulated after CIA immunizations compared to thenormal rats (**Figure 4E**). However, WJT treatment significantly reversed the trend.

WJT manipulates the metabolic patterns

Our metabolomic analysis, based on UHPLC-MS/MS, detected a total of 522 metabolites in negative mode and 707 metabolites in positive mode. Volcano plots depicting differentially abundant metabolites among groups revealed that there were 177 and 151 differentiated metabolites between control and model groups, and model and WJT treatment groups, respectively (**Supplymentary Figure S2A)**. More details were shown in **Supplymentary TableS 2.** In addition, heatmaps were used to display the relative levels of the differentiated metabolites among groups(**Supplymentary Figure S2B).**

KEGG analysis was conducted to reveal the significantly enriched pathways by differentiated metabolites among different groups (**Figure 5A and B**). More details were shown in **Supplymentary Table S3 and S4. T**he abundances of metabolites in these correspondingly enriched pathways were statistically analyzed (**Figure 5C and D**). Com_643_pos (Serotonin), Com_1623_pos (Glutathione disulfide), Com_5570_pos (N-Acetylneuraminic acid), Com_3187_pos (Naphthalene) and Com_520_pos (Thromboxane B2) were tended to be reversed by WJT compared to the CIA rats. These five metabolites might be involved in the therapeutic treatment of WJT for RA, and more information about the five metabolites was shown in **Supplymentary Table S5.**

Correlation analysis and ROC curve

The metabolites associated with the special bacterial genera (*Vibrio*, *Macrococcus* and *Vagococcus*) were identified by Pearson correlation analysis (Figure 6A), and the relative abundances of these special metabolites were statistically analyzed according to metabolomic analyses (Figure 6B). The abundances of Com_5483_pos (3'-N-debenzoyl-2'-deoxytaxol), Com_1491_pos (Tubulysin B), Com_4251_pos (Dexamethasone cipecilate), Com_3042_neg (Magnoline) and Com_1330_neg (Hydrocortisone Valerate) were significantly reversed by WJT treatment compared to the CIA rats. ROC analysis confirmed that these five differentiated metabolites had AUC values ranging from 0.90 to 0.97, indicating these compounds might also be potential targets of WJT treatment for RA (Supplymentary Figure S3). In addition, more information about the five metabolites was shown in Supplymentary Table S5.

Discussion

Rheumatoid arthritis (RA) characterized by joint swelling, synovial inflammation, and cartilage and bone destruction, is a chronic autoimmune disease that impairs joint movements [2]. An increasing number of RA patients and those with other diseases are selecting natural products to satisfy their healthcare needs [18]. WJT is a type of traditional Chinese medicine (TCM) that is a mixture of herbal compounds, and has been used for clinical treatments for many years. In this study, we mainly investigated the anti-inflammatory and pharmacological effects of WJT on CIA rats to identify its pharmacological targets and potential molecular mechanisms, and the therapeutic mechanism of WJT for RA was elucidated in **Supplymentary Figure S4.**

The results of clinical manifestations and pathological changes demonstrated that WJT played an important role in suppressing the pathological progression of arthritis in CIA rats, which laid a foundation

for the further study. In addition, The aberrant release and recruitment of pro-inflammatory cytokines (TNF-α, IL-1β, and IL-6) are essential to the pathogenesis of RA [17, 29, 20]. It's well known that both TNF-α and IL-1β play roles in the activation and infiltration of immune cells, and contribute to production of inflammatory cytokines and chemokines, thereby resulting in a complex network that promotes inflammatory reactions, cartilage damage and autoimmune pathology [17, 21]. Moreover, IL-6 acts on B lymphocytes and helps them to release many pro-inflammatory molecules around the joints [22]. It also up-regulates the sensitivity of the osteoclasts and promotes the activation of the fibroblast synovial cells, thereby contributing to synovial pannus formation and cartilage destruction [4]. Our results indicated that WJT down-regulated the levels of these pro-inflammatory cytokines in serum and joint tissue. Thus, the therapeutic mechanisms of WJT for RA appears related to its inhibition of pro-inflammatory cytokines.

In this study, our results showed that WJT significantly altered the overall structure of gut microbiota in CIA rats. *Firmicutes* and *Bacteroidetes* were the two most abundant bacterial phyla in the gut microbiota community. A common metabolite of Gram-positive *Firmicutes*, butyrate, is identified as an anti-inflammatory molecule, which help to impede bacterial transport across the intestinal epithelial wall and increase the rate of tight junction formation, thereby maintaining the healthy gut environment [23, 24]. The aberrant proliferation of Gram-negative *Bacteroidetes* contributes to the production of lipopolysaccharides (LPS) and then induces the low-grade inflammation by activating Toll-like receptor 4 (TLR-4) [25]. In addition, *Bacteroidetes* can increase intestinal permeability and promote a chronic inflammatory state by degrading mucin on the intestinal membrane [26]. The ratio of *Bacteroidetes* to *Firmicutes* was up-regulated in many autoimmune diseases, such as type 1 diabetes mellitus (T1DM), systemic *lupus erythematosus* (SLE), and so on [23]. In this study, the high ratio of *Bacteroidetes* to *Firmicutes* in CIA rats was prominently reversed by WJT treatment, which might be a therapeutic mechanism of WJT for RA.

At the genus level, the CIA rats significantly increased the number of *Vibrio*, *Macrococcus*, and *Vagococcus*. However, WJT supplement recovered these bacterial genera, *Vibrio*, a highly motile Gram-negative bacteria of the phylum *Proteobacteria*, is correlated with human diseases, such as cholera, vibriosis, wound infections, and so on [27]. Additionally, *Vibrio* increasing the levels of IL-6 and TNF-α induces the inflammatory responses RAW264.7 macrophages and causes inflammation in vivo [21]. From the point of view, that WJT decreased *Vibrio* population might be associated with the reduction of pro-inflammatory cytokines levels in serum and ankle tissue. Both *Macrococcus* and *Vagococcus* are the members of the phylum *Firmicutes*. It is accepted that *Macrococcus* is involved in the inflammatory infiltration, hemorrhages, multifocal necrosis of various organs, and pathological changes of caseous exudation in cranial cavities [28]. In addition, a recent study revealed that *Vagococcus* modulating the inflammatory responses induced the neuropsychiatric disorders [29]. Therefore, we hypothesize that WJT supplement is beneficial to normalize these bacteria close to the normal level, thereby recovering the pathogenesis in CIA rats.

In this work, WJT trended to restore the abundances of serotonin, glutathione disulfide, N-acetylneuraminic acid, naphthalene and thromboxane B2 in CIA rats, and the signaling pathways and the

functions of these five metabolites associated with RA were illustrated in **Supplymentary Figure S4**, which was another therapeutic mechanism of WJT for RA.

3'-N-debenzoyl-2'-deoxytaxol, dexamethasone cipecilate, tubulysin B, magnoline, and hydrocortisone valerate were another five metabolites identified by correlation analysis, which were prominently reversed by WJT in CIA rats. Dexamethasone cipecilate characterized by increasing lipophilicity and enhancing pharmacological action has been identified as an effective therapy for allergic rhinitis [30]. Magnoline, an anti-inflammatory compound, has ability to inhibit the proliferation of cancer cells [31, 32]. Meanwhile, tubulysins also exhibits anti-proliferative effects on cancer cell [33]. And hydrocortisone valerate is another metabolite molecule correlated with low-grade inflammation [34]. 3'-N-debenzoyl-2'-deoxytaxol has not been reported in pharmacology until now. Thus, these findings suggest that the special metabolites might be therapeutic targets of WJT for RA.

Conclusion

In this study, our results indicated that WJT restored the paw swelling, reversed the levels of inflammatory cytokines, inhibited the MEK/ERK signaling , and induced synoviocyte apoptosis. Additionally, it prominently altered the overall gut microbial structure of CIA rats. The ratio of *Bacteroidetes* to *Firmicutes*, and the abundances of bacterial genera (*Vibrio*, *Macrococcus* and *Vagococcus*) significantly reversed after WJT treatment in CIA rats. These findings might be the therapeutic mechanisms of WJT for RA. Moreover, serotonin, glutathione disulfide, N-acetylneuraminic acid, naphthalene, thromboxane B 2, 3'-N-debenzoyl-2'-deoxytaxol, dexamethasone cipecilate, tubulysin B, magnoline, and hydrocortisone valerate also might be therapeutic targets of WJT for RA. Our results provide a basis for its safe and effective administration in clinical practice. However, a systematic and comprehensive interpretation of the therapeutic effect of WJT on RA requires further investigation.

List Of Abbreviations

WJT, Wantong Jingu Tablet; RA, rheumatoid arthritis; CIA, collagen-induced arthritis; AI, arthritis index; LC-MS, liquid chromatograph-mass spectrometer; PCoA, principal co-ordinates analysis; LD50, the median lethal dose; UPGMA, Unweighted pair-group method with arithmetic means; OTUs, operational taxonomic units; KEGG, kyoto encyclopedia of genes and genomes; TCM, traditional Chinese medicine; ROC, receiver operating characteristic; AUC, area under ROC curve; ESI+, positive electrospray ionization mode; ESI-, negative electrospray ionization mode.

Declarations

Ethics approval and consent to participate

All animal experiments were approved by the Animal Research Committee of Jilin University. The principles in the ARRIVE guidelines and the Basel declaration (http://www.basel.declaration.org) have

been considered when planning the experiments.

Consent for publication

This manuscript is approved by all authors for publication.

Availability of data and materials

The datasets generated for this study are available on request to the corresponding author.

Competing interests

The authors declare no Competing interests.

Funding

Author Contributions

FL and ZL conceived and designed the experiments; ZL and FQ performed the experiments; ZL and FQ carried out the statistical analysis; GW and ZL wrote the paper. All authors have read and approved the manuscript.

Acknowledgments

References

1. Xing R, Jin Y, Sun L, et al. Interleukin-21 induces migration and invasion of fibroblast-like synoviocytes from patients with rheumatoid arthritis. Clin Exp Immunol. 2016;184:147-58.
2. Liu W, Zhang Y, Zhu W, et al. Sinomenine Inhibits the Progression of Rheumatoid Arthritis by Regulating the Secretion of Inflammatory Cytokines and Monocyte/Macrophage Subsets. Front Immunol. 2018;9:2228.

3. Bartok B, Firestein GS. Fibroblast-like synoviocytes: key effector cells in rheumatoid arthritis. Immunol Rev. 2010;233:233-55.

4. Rana AK, Li Y, Dang Q, Yang F. Monocytes in rheumatoid arthritis: Circulating precursors of macrophages and osteoclasts and, their heterogeneity and plasticity role in RA pathogenesis. Int Immunopharmacol. 2018;65:348-59.

5. Merola JF, Espinoza LR, Fleischmann R. Distinguishing rheumatoid arthritis from psoriatic arthritis. RMD Open. 2018;4:e000656.

6. Zhao SJ, Fan L, Wang BX, et al. Zhuanggu Yisui Granules in treating cervical spondylotic myelopathy [in China]. Journal of Changchun University of Chinese Medicine. 2015;31:143-5.

7. Xiong MY, lu XL, Liu ZH, et al. Clinical observation of Wantong Jingu Tablets combined with triamcinolone acetonide in treatment of periarthritis [in China]. Drugs & Clinic. 2017;32:702-5.

8. Wang JY, Zhang TY, Qiao XF, et al. Effects of three drugs on apoptosis and gene expression of synovial cells in CIA rats [in China]. Heilongjiang Medicine and Pharmacy. 2015;38:76-7.

9. Zhu HZ, Liang YD, Ma QY, et al. Xiaoyaosan improves depressive-like behavior in rats with chronic immobilization stress through modulation of the gut microbiota. Biomed Pharmacother. 2019;112:108621.

10. Pferschy-Wenzig EM, Koskinen K, Moissl-Eichinger C, et al. A Combined LC-MS Metabolomics- and 16S rRNA Sequencing Platform to Assess Interactions between Herbal Medicinal Products and Human Gut Bacteria in Vitro: a Pilot Study on Willow Bark Extract. Front Pharmacol. 2017;8:893.

11. Furukawa H, Oka S, Shimada K, et al. Serum Metabolomic Profiles of Rheumatoid Arthritis Patients With Acute-Onset Diffuse Interstitial Lung Disease. Biomark Insights. 2019;14:1177271919870472.

12. Dai Q, Zhou D, Xu L, et al. Curcumin alleviates rheumatoid arthritis-induced inflammation and synovial hyperplasia by targeting mTOR pathway in rats. Drug Des Devel Ther. 2018;12:4095-105.

13. Wang K, Zhang D, Liu Y, et al. Traditional Chinese medicine formula Bi-Qi capsule alleviates rheumatoid arthritis-induced inflammation, synovial hyperplasia, and cartilage destruction in rats. Arthritis Res Ther. 2018;20:43.

14. Zuo J, Wang X, Liu Y, et al. Integrating Network Pharmacology and Metabolomics Study on Anti-rheumatic Mechanisms and Antagonistic Effects Against Methotrexate-Induced Toxicity of Qing-Luo-Yin. Front Pharmacol. 2018;9:1472.

15. Haleagrahara N, Hodgson K, Miranda-Hernandez S, et al. Flavonoid quercetin-methotrexate combination inhibits inflammatory mediators and matrix metalloproteinase expression, providing protection to joints in collagen-induced arthritis. Inflammopharmacology. 2018;26:1219-32.

16. Balkrishna A, Sakat SS, Joshi K, et al. Anti-Inflammatory and Anti-Arthritic Efficacies of an Indian Traditional Herbo-Mineral Medicine "Divya Amvatari Ras" in Collagen Antibody-Induced Arthritis (CAIA) Mouse Model Through Modulation of IL-6/IL-1beta/TNF-alpha/NFkappaB Signaling. Front Pharmacol. 2019;10:659.

17. Wang J, Feng W, Zhang S, et al. Gut microbial modulation in the treatment of chemotherapy-induced diarrhea with Shenzhu Capsule. BMC Complement Altern Med. 2019;19:126.

18. Dudics S, Langan D, Meka RR, et al. Natural Products for the Treatment of Autoimmune Arthritis: Their Mechanisms of Action, Targeted Delivery, and Interplay with the Host Microbiome. Int J Mol Sci. 2018;19(9):2508.

19. Du H, Zhang X, Zeng Y, et al. A Novel Phytochemical, DIM, Inhibits Proliferation, Migration, Invasion and TNF-alpha Induced Inflammatory Cytokine Production of Synovial Fibroblasts From Rheumatoid Arthritis Patients by Targeting MAPK and AKT/mTOR Signal Pathway. Front Immunol. 2019;10:1620.

20. Wang J, Zhao Q. Kaempferitrin inhibits proliferation, induces apoptosis, and ameliorates inflammation in human rheumatoid arthritis fibroblast-like synoviocytes. Phytother Res. 2019;33:1726-35.

21. Qin K, Fu K, Liu J, et al. Vibrio vulnificus cytolysin induces inflammatory responses in RAW264.7 macrophages through calcium signaling and causes inflammation in vivo. Microb Pathog. 2019;137:103789.

22. Niu Q, Huang ZC, Wu XJ, et al. Enhanced IL-6/phosphorylated STAT3 signaling is related to the imbalance of circulating T follicular helper/T follicular regulatory cells in patients with rheumatoid arthritis. Arthritis Res Ther. 2018;20:200.

23. Kasselman LJ, Vernice NA, DeLeon J, et al. The gut microbiome and elevated cardiovascular risk in obesity and autoimmunity. Atherosclerosis. 2018;271:203-13.

24. Kim JA, Kim SH, Kim IS, et al. Anti-Inflammatory Effects of a Mixture of Lactic Acid Bacteria and Sodium Butyrate in Atopic Dermatitis Murine Model. J Med Food. 2018;21:716-25.

25. Graham C, Mullen A, Whelan K. Obesity and the gastrointestinal microbiota: a review of associations and mechanisms. Nutr Rev. 2015;73:376-85.

26. Brown CT, Davis-Richardson AG, Giongo A, et al. Gut microbiome metagenomics analysis suggests a functional model for the development of autoimmunity for type 1 diabetes. PLoS One. 2011;6:e25792.

27. Echazarreta MA, Klose KE. Vibrio Flagellar Synthesis. Front Cell Infect Microbiol. 2019;9:131.

28. Li G, Du X, Zhou D, et al. Emergence of pathogenic and multiple-antibiotic-resistant Macrococcus caseolyticus in commercial broiler chickens. Transbound Emerg Dis. 2018;65:1605-14.

29. Sun L, Zhang H, Cao Y, et al. Fluoxetine ameliorates dysbiosis in a depression model induced by chronic unpredicted mild stress in mice. Int J Med Sci. 2019;16:1260-70.

30. Sasagawa T, Yamada T, Nakagawa T, et al. In vitro metabolism of dexamethasone cipecilate, a novel synthetic corticosteroid, in human liver and nasal mucosa. Xenobiotica. 2011;41:874-84.

31. Sun H, Zhang AH, Liu SB, et al. Cell metabolomics identify regulatory pathways and targets of magnoline against prostate cancer. J Chromatogr B Analyt Technol Biomed Life Sci. 2018;1102-1103:143-51.

32. Zhou Y, Wang F, Hao L, et al. Effects of magnoline on P-selectin's expression in diabetic rats and its reno-protection. Kidney Blood Press Res. 2013;37:211-20.

33. Draca D, Mijatovic S, Krajnovic T, et al. Synthetic Tubulysin Derivative, Tubugi-1, Against Invasive Melanoma Cells: The Cell Death Triangle. Anticancer Res. 2019;39:5403-15.

34. Martocchia A, Gallucci M, Noale M, et al. The cortisol burden in elderly subjects with metabolic syndrome and its association with low-grade inflammation. Aging Clin Exp Res. 2019; doi:10.1007/s40520-019-01322-3.
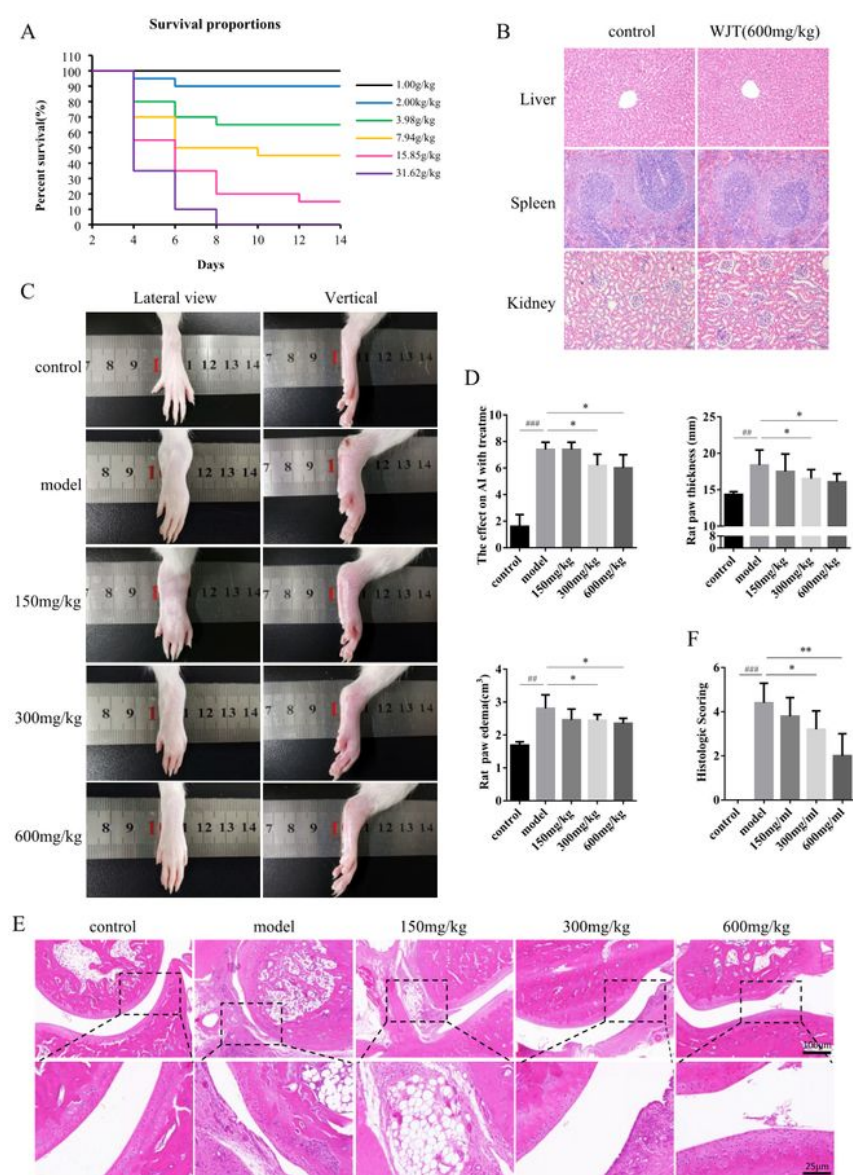
Figures

Figure 1

Effect of WJT on the development and progression of CIA in rats. (A) Survival curves of healthy rats given different single doses of WJT. (LD50: 6.24 g/kg, 95% CI: 4.16, 9.34). (B) H&E staining results showed no significant organ related toxicities. (C) Representative images of the hind paws of rats. (D) Arthritis clinical score, paw thickness, and paw edema of the hind paws of rats. (E and F) H&E staining and histologic scoring of ankle joints of rats. WJT, Wantong Jingu Tablet; CIA, collagen-induced rheumatoid
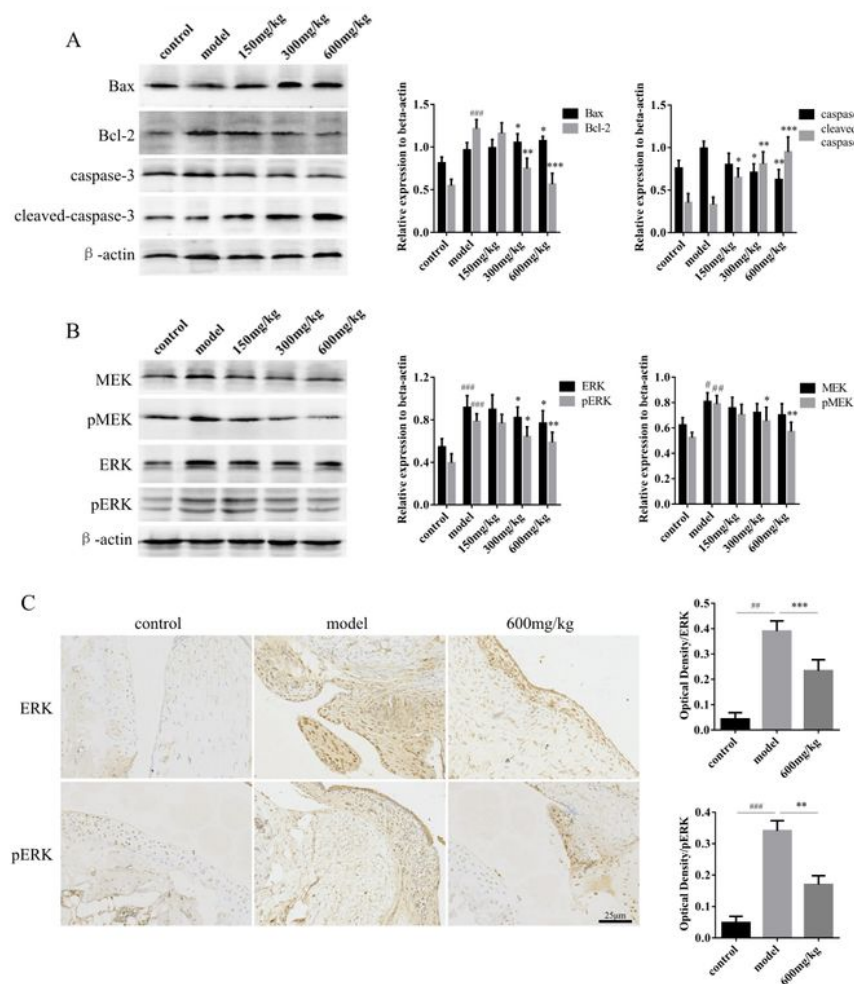
Figure 2

Effect of WJT on synovial tissues of rats with CIA. (A) Effect of WJT on the levels of synovial proteins in mitochondrial apoptosis pathway. (B) Western blotting of proteins in the ERK/pERK pathway in synovial tissues. (C) IHC staining of ERK and pERK in the synovial tissues. Values were expressed as mean ± SD

(n = 10). #p<0.05, ##p<0.01, ###p<0.001 vs. control group; *p<0.05, **p<0.01, ***p<0.001 vs. model group.
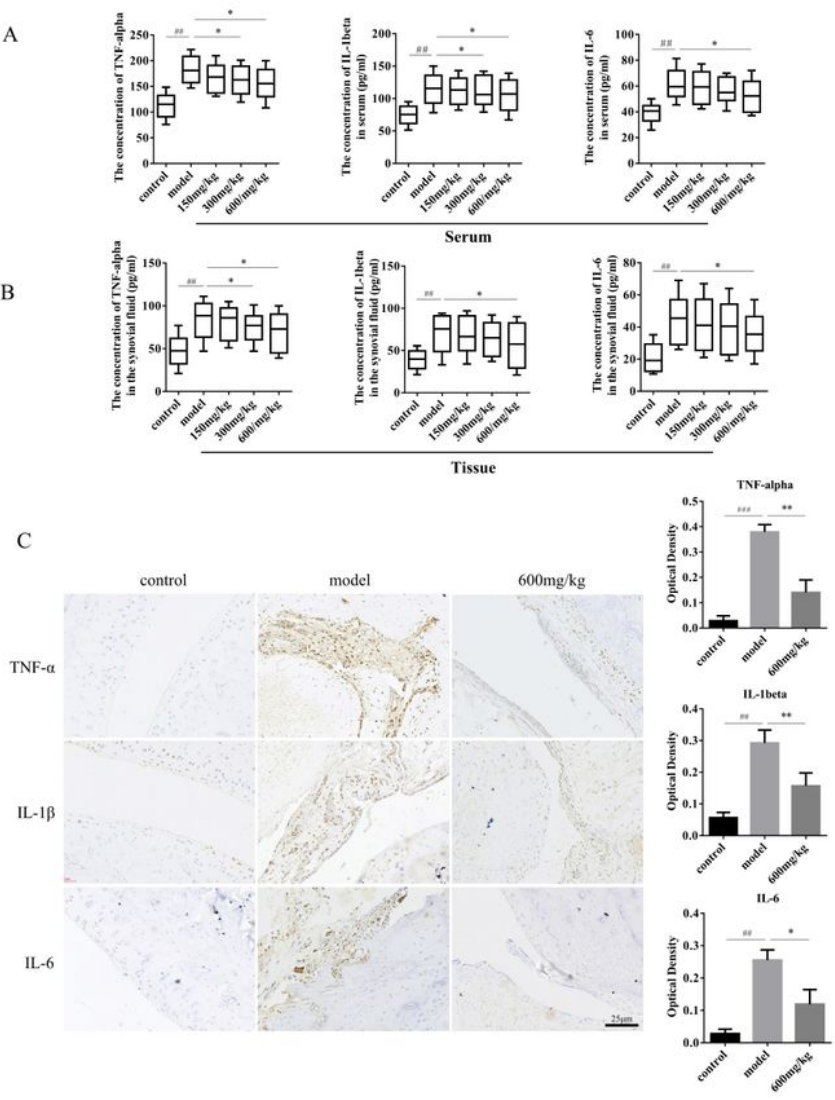

Figure 3

Effect of WJT on production of pro-inflammatory cytokines in rats with CIA. (A) Serum levels of TNF-α, IL-1β, and IL-6, measured using ELISA. (B and C) Ankle tissue levels of TNF-α, IL-1β, and IL-6, measured

using ELISA and immunohistochemical staining. Values were expressed as mean ± SD (n = 10). ##p<0.01, ###p<0.001 vs. control group; *p<0.05, **p<0.01 vs. model group.
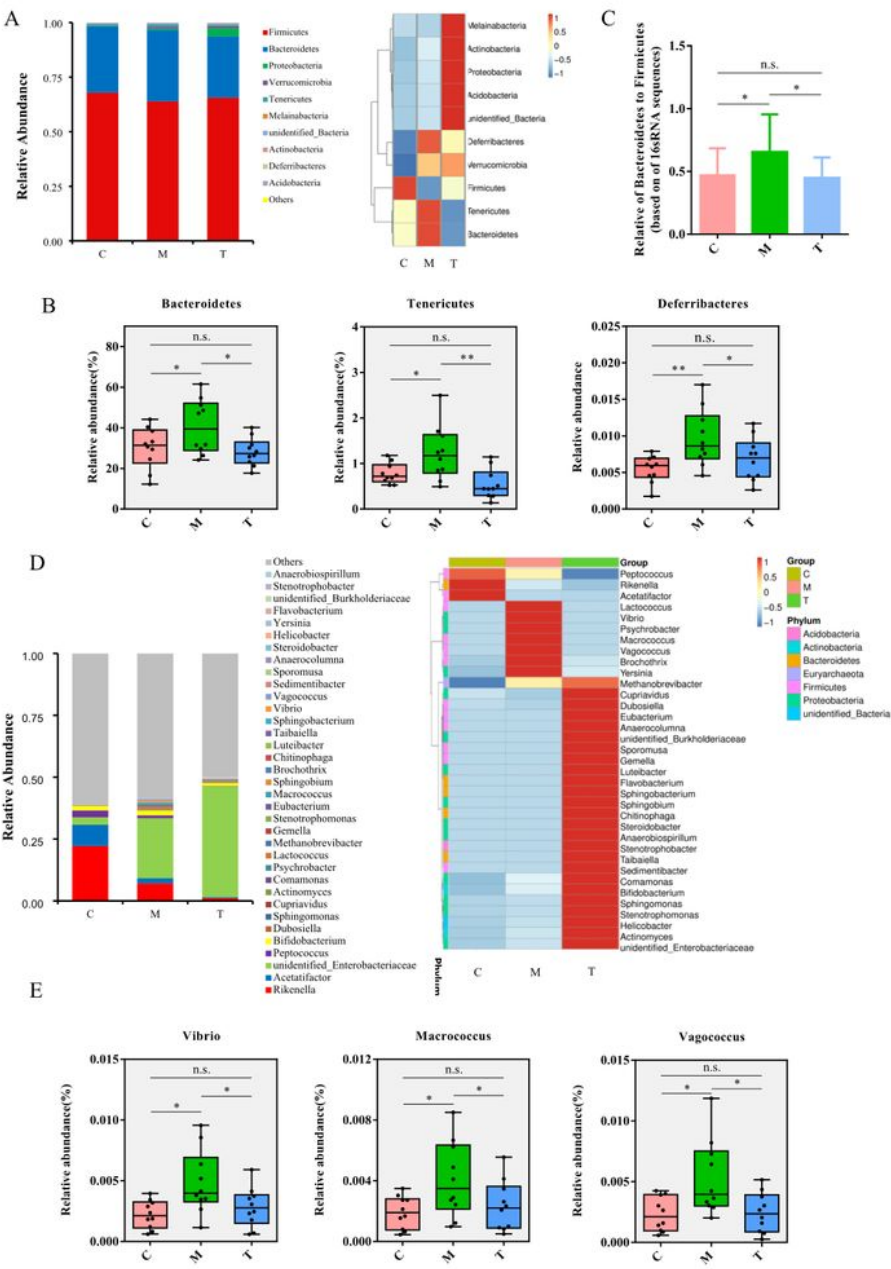

Figure 4

Effect of WJT on the composition of gut microbiota in rats with CIA. (A) Relative abundance and clustering map of the dominant bacterial phyla. (B) WJT reversed the specific bacterial phyla. (C) The ratio of Bacteroidetes to Firmicutes. (D) Relative abundance and clustering map of the dominant bacterial

genera. (E) WJT reversed the specific bacterial genera.Values were expressed as mean ± SD. n = 10 per group. *p < 0.05; **p < 0.01; n.s., no significance.
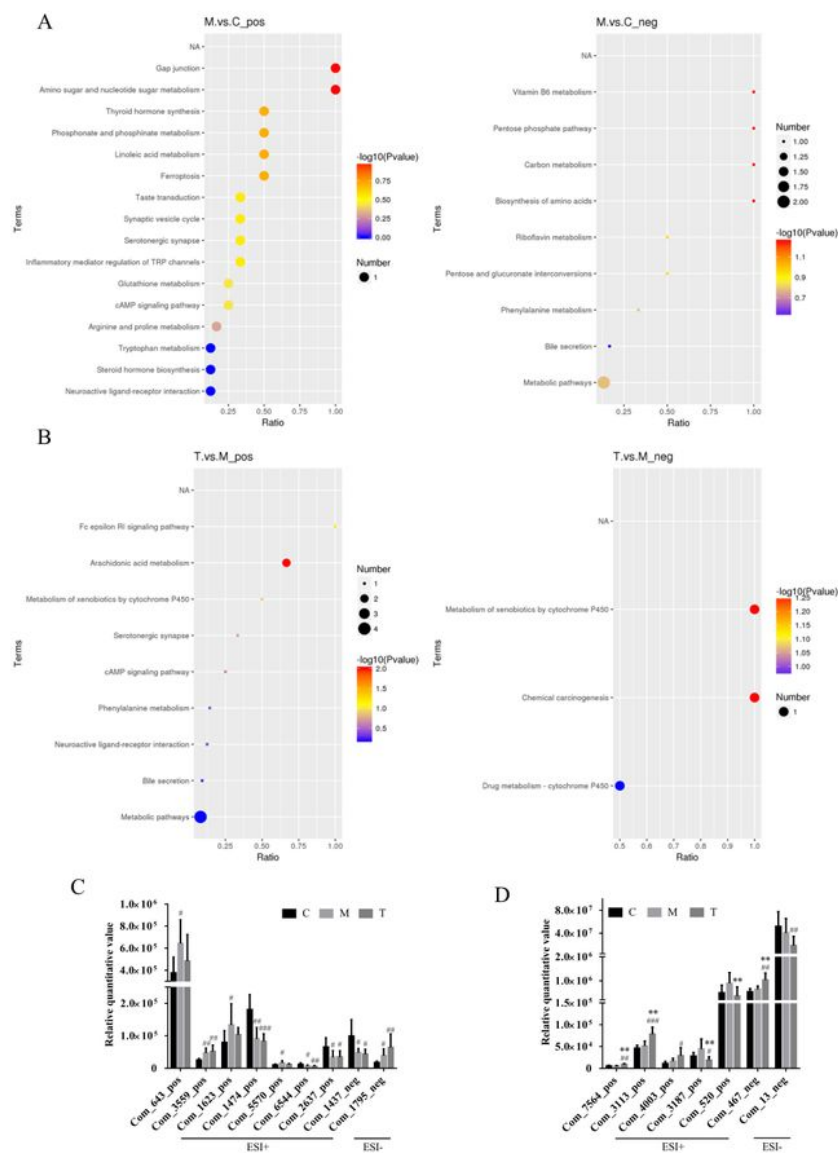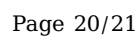

Figure 5

Identification of the differential metabolites in fecal samples. (A and B) KEGG enrichment analysis of differentiated metabolites among the different groups. Statistical analysis of the differentiated metabolites significantly enriching in KEGG pathways among control and model groups (C), and model

and WJT treatment groups (D). WJT tended to reverse five specific metabolites: Com_643_pos, Com_1623_pos, Com_5570_pos, Com_3187_pos and Com_520_pos. Values were expressed as mean ± SD. n = 10 per group. #p< 0.05, ##p < 0.01, ###p< 0.001 vs. C (control); *p < 0.05, **p < 0.01 vs. M (model).

Figure 6

Correlation analysis of the specific bacterial genera with different metabolites. (A) Pearson correlation heatmaps for the two indicated groups in ESI+ and ESI- modes. (B) Quantitative analysis of specific metabolites associated with Vibrio, Macrococcus and Vagococcus, and WJT reversed the five specific metabolites: Com_5483_pos, Com_4251_pos, Com_1491_pos, Com_3042_neg and Com_1330_neg. Values were expressed as mean ± SD. n = 10 per group. *p < 0.05, **p < 0.01; n.s., no significance.

Supplementary Files

This is a list of supplementary files associated with this preprint. Click to download.

- SupplymentaryFile.pdf